Search for *CP* violation in $\Xi_c^+ \to \Sigma^+ h^+ h^-$ and $\Lambda_c^+ \to p h^+ h^-$ at Belle II

M. Abumusabh, I. Adachi, H. Ahmed, Y. Ahn, H. Aihara, N. Akopov, S. Alghamdi, M. Alhakami, N. Althubiti, K. Amos, N. Anh Ky, D. M. Asner, H. Atmacan, R. Ayad, V. Babu, N. K. Baghel, S. Bahinipati, P. Bambade, Sw. Banerjee, M. Bartl, J. Baudot, A. Beaubien, J. Becker, J. V. Bennett, V. Bertacchi, M. Bertemes, E. Bertholet, S. Bettarini, V. Bhardwaj, D. Biswas, A. Bobrov, D. Bodrov, G. Bonvicini, J. Borah, A. Boschetti, M. Bračko, P. Branchini, R. A. Briere, T. E. Browder, A. Budano, S. Bussino, Q. Campagna, M. Campajola, G. Casarosa, C. Cecchi, P. Chang, P. Cheema, L. Chen, B. G. Cheon, C. Cheshta, H. Chetri, K. Chilikin, J. Chin, K. Chirapatpimol, H.-E. Cho, K. Cho, S.-J. Cho, S.-K. Choi, S. Choudhury, S. Chutia, J. A. Colorado-Caicedo, I. Consigny, L. Corona, J. X. Cui, S. Das, S. A. De La Motte, G. De Nardo, G. De Pietro, R. de Sangro, M. Destefanis, A. Di Canto, Z. Doležal, I. Domínguez Jiménez, T. V. Dong, X. Dong, M. Dorigo, G. Dujany, P. Ecker, D. Epifanov, J. Eppelt, R. Farkas, P. Feichtinger, T. Ferber, T. Fillinger, G. Finocchiaro, F. Forti, B. G. Fulsom, A. Gabrielli, E. Ganiev, R. Garg, G. Gaudino, V. Gaur, V. Gautam, A. Gaz, A. Gellrich, D. Ghosh, H. Ghumaryan, R. Giordano, A. Giri, P. Gironella Gironell, A. Glazov, B. Gobbo, R. Godang, O. Gogota, P. Goldenzweig, W. Gradl, E. Graziani, D. Greenwald, K. Gudkova, I. Haide, Y. Han, S. Hazra, M. T. Hedges, A. Heidelbach, G. Heine, I. Heredia de la Cruz, M. Hernández Villanueva, D. Hettiarachchi, T. Higuchi, M. Hoek, M. Hohmann, R. Hoppe, P. Horak, X. T. Hou, C.-L. Hsu, T. Humair, T. Iijima, N. Ipsita, A. Ishikawa, R. Itoh, M. Iwasaki, W. W. Jacobs, D. E. Jaffe, E.-J. Jang, S. Jia, Y. Jin, A. Johnson, A. B. Kaliyar, J. Kandra, K. H. Kang, G. Karyan, F. Keil, C. Kiesling, D. Y. Kim, J.-Y. Kim, K.-H. Kim, K. Kinoshita, P. Kodyš, T. Koga, S. Kohani, A. Korobov, S. Korpar, E. Kovalenko, R. Kowalewski, P. Križan, P. Krokovny, T. Kuhr, K. Kumara, T. Kunigo, A. Kuzmin, Y.-J. Kwon, S. Lacaprara, T. Lam, T. S. Lau, M. Laurenza, R. Leboucher, F. R. Le Diberder, H. Lee, M. J. Lee, C. Lemettais, P. Leo, P. M. Lewis, C. Li, L. K. Li, Q. M. Li, W. Z. Li, Y. Li, Y. B. Li, Y. P. Liao, J. Libby, J. Lin, S. Lin, M. H. Liu, Q. Y. Liu, Z. Liu, D. Liventsev, S. Longo, T. Lueck, C. Lyu, J. L. Ma, Y. Ma, M. Maggiora, R. Manfredi, E. Manoni, M. Mantovano, D. Marcantonio, M. Marfoli, C. Marinas, C. Martellini, A. Martens, T. Martinov, L. Massaccesi, M. Masuda, D. Matvienko, S. K. Maurya, M. Maushart, J. A. McKenna, Z. Mediankin Gruberová, F. Meier, D. Meleshko, M. Merola, C. Miller, M. Mirra, K. Miyabayashi, R. Mizuk, G. B. Mohanty, S. Moneta, A. L. Moreira de Carvalho, H.-G. Moser, M. Mrvar, H. Murakami, I. Nakamura, M. Nakao, Y. Nakazawa, M. Naruki, Z. Natkaniec, A. Natochii, M. Nayak, M. Neu, S. Nishida, R. Nomaru, S. Ogawa, H. Ono, G. Pakhlova, A. Panta, S. Pardi, J. Park, S.-H. Park, A. Passeri, S. Patra, S. Paul, T. K. Pedlar, R. Pestotnik, L. E. Piilonen, P. L. M. Podesta-Lerma, T. Podobnik, C. Praz, S. Prell, E. Prencipe, M. T. Prim, H. Purwar, P. Rados, S. Raiz, K. Ravindran, J. U. Rehman, M. Reif, S. Reiter, L. Reuter, D. Ricalde Herrmann, I. Ripp-Baudot, G. Rizzo, J. M. Roney, A. Rostomyan, N. Rout, L. Salutari, D. A. Sanders, S. Sandilya, L. Santelj, C. Santos, B. Scavino, C. Schmitt, M. Schnepf, K. Schoenning, C. Schwanda, Y. Seino, K. Senyo, M. E. Sevior, C. Sfienti, W. Shan, G. Sharma, X. D. Shi, T. Shillington, J.-G. Shiu, D. Shtol, B. Shwartz, A. Sibidanov, F. Simon, J. Skorupa, R. J. Sobie, M. Sobotzik, A. Soffer, A. Sokolov, S. Spataro, B. Spruck, M. Starič, P. Stavroulakis, R. Stroili, M. Sumihama, M. Takahashi, U. Tamponi, S. S. Tang, K. Tanida, F. Tenchini, A. Thaller, T. Tien Manh, O. Tittel, R. Tiwary, E. Torassa, K. Trabelsi, F. F. Trantou, I. Ueda, K. Unger, Y. Unno, K. Uno, S. Uno, P. Urquijo, Y. Ushiroda, R. van Tonder, K. E. Varvell, M. Veronesi, V. S. Vismaya, L. Vitale, V. Vobbilisetti, R. Volpe, M. Wakai, S. Wallner, M.-Z. Wang, A. Warburton, S. Watanuki, C. Wessel, E. Won, X. P. Xu, B. D. Yabsley, W. Yan, K. Yi, J. H. Yin, K. Yoshihara, J. Yuan, Y. Yusa, L. Zani, F. Zeng, B. Zhang, V. Zhilich, J. S. Zhou, Q. D. Zhou, L. Zhu, and R. Žlebčík

(Belle II Collaboration)

(Received 1 October 2025; accepted 22 January 2026; published 24 February 2026)

We report decay-rate CP asymmetries of the singly-Cabibbo-suppressed decays $\Xi_c^+ \to \Sigma^+ h^+ h^-$ and $\Lambda_c^+ \to p h^+ h^-$, with $h = K$, π, measured using 428 fb^{-1} of e^+e^- collisions collected by the Belle II experiment at the SuperKEKB collider. The results, $A_{CP}(\Xi_c^+ \to \Sigma^+ K^+ K^-) = (3.7 \pm 6.6 \pm 0.6)\%$, $A_{CP}(\Xi_c^+ \to \Sigma^+ \pi^+ \pi^-) = (9.5 \pm 6.8 \pm 0.5)\%$, $A_{CP}(\Lambda_c^+ \to p K^+ K^-) = (3.9 \pm 1.7 \pm 0.7)\%$, $A_{CP}(\Lambda_c^+ \to p \pi^+ \pi^-) = (0.3 \pm 1.0 \pm 0.2)\%$, where the first uncertainties are statistical and the second systematic, agree with CP symmetry. From these results we derive the sums $A_{CP}(\Xi_c^+ \to \Sigma^+ \pi^+ \pi^-) + A_{CP}(\Lambda_c^+ \to p K^+ K^-) = (13.4 \pm 7.0 \pm 0.9)\%$, $A_{CP}(\Xi_c^+ \to \Sigma^+ K^+ K^-) + A_{CP}(\Lambda_c^+ \to p \pi^+ \pi^-) = (4.0 \pm 6.6 \pm 0.7)\%$, which are consistent with the U-spin symmetry prediction of zero. These are the first measurements of CP asymmetries for individual hadronic three-body charmed-baryon decays.

DOI: 10.1103/s2gy-c3vh

I. INTRODUCTION

Violation of charge-parity (CP) symmetry has been established in decays of strange, charmed, and bottom mesons [1–11] and recently bottom baryons [12]. The LHCb Collaboration established CP violation in charm decays by observing a nonzero difference between the decay-rate CP asymmetries of $D^0 \to K^+K^-$ and $D^0 \to \pi^+\pi^-$ [10]. (Charge-conjugate modes are included implicitly.) The standard model explains the measured CP asymmetries of strange and bottom decays (see, for example, Sections 12 and 13 of Ref. [13]), yet offers no clear interpretation of the CP asymmetry measured for charm decays. Some theoretical interpretations have suggested the measured CP asymmetry of order 10^{-3} arises from interactions beyond the standard model [14–20], others from nonperturbative QCD [21–25]. Moreover, LHCb's separate determinations of $A_{CP}(D^0 \to K^+K^-)$ and $A_{CP}(D^0 \to \pi^+\pi^-)$ [11] indicate unexpectedly large breaking of U-spin symmetry [26], which assumes invariance under the exchange of down and strange quarks and predicts that the CP asymmetries of $D^0 \to K^+K^-$ of and $D^0 \to \pi^+\pi^-$ have equal magnitudes and opposite signs [27,28].

Another place to search for CP violation and test U-spin symmetry is in three-body, singly Cabibbo-suppressed, hadronic charmed-baryon decays [29,30]. Assuming U-spin symmetry,

$$A_{CP}(\Xi_c^+ \to \Sigma^+ \pi^+ \pi^-) + A_{CP}(\Lambda_c^+ \to p K^+ K^-) = 0, \quad (1)$$

$$A_{CP}(\Xi_c^+ \to \Sigma^+ K^+ K^-) + A_{CP}(\Lambda_c^+ \to p \pi^+ \pi^-) = 0. \quad (2)$$

None of these asymmetries have been measured, individually or in these sums, despite the large branching fractions of their decays. LHCb measured the difference between $A_{CP}(\Lambda_c^+ \to p K^+ K^-)$ and $A_{CP}(\Lambda_c^+ \to p \pi^+ \pi^-)$ [31], but since they are not related by U-spin this does not reveal anything about U-spin-symmetry breaking.

We report the first measurements of the CP asymmetries of $\Xi_c^+ \to \Sigma^+ h^+ h^-$ and $\Lambda_c^+ \to p h^+ h^-$, with $h = K$, π. We use 428 fb^{-1} of e^+e^- collisions collected at or near the $\Upsilon(4S)$ center-of-mass energy by the Belle II experiment from 2019 to 2022.

The decay-rate CP asymmetry of charmed baryon X_c^+ decaying to final state f^+ is

$$A_{CP}(X_c^+ \to f^+) \equiv \frac{\Gamma(X_c^+ \to f^+) - \Gamma(\bar{X}_c^- \to \bar{f}^-)}{\Gamma(X_c^+ \to f^+) + \Gamma(\bar{X}_c^- \to \bar{f}^-)}. \quad (3)$$

We determine it by measuring the asymmetry of yields,

$$A_N(X_c^+ \to f^+) \equiv \frac{N(X_c^+ \to f^+) - N(\bar{X}_c^- \to \bar{f}^-)}{N(X_c^+ \to f^+) + N(\bar{X}_c^- \to \bar{f}^-)}, \quad (4)$$

which we correct for detection and production asymmetries. In the limit of small asymmetries,

$$A_N(X_c^+ \to f^+) = A_{CP}(X_c^+ \to f^+) + A_{\rm p}(X_c^+) + A_{\rm d}(f^+), \quad (5)$$

where $A_{\rm p}(X_c^+)$ is due to the forward-backward asymmetry of charmed-baryon production in e^+e^- collisions [32–34] and $A_{\rm d}(f^+)$ is the asymmetry of detecting the charged final-state particles.

Since $A_{\rm p}$ is an odd function of the cosine of the polar angle of the charmed baryon's momentum in the e^+e^- center-of-mass (c.m.) frame, $\cos\theta$, we suppress it by replacing A_N in Eq. (4) with the average of the A_N measured separately in the forward and backward regions,

$$A_N' = \frac{A_N(\cos\theta > 0) + A_N(\cos\theta < 0)}{2}. \quad (6)$$

We remove the charged-particle detection asymmetries by subtracting the yield asymmetries of control channels, $\Lambda_c^+ \to \Sigma^+ h^+ h^-$, $\Lambda_c^+ \to p \pi^+ K^-$, and $D^0 \to \pi^+ K^- \pi^+ \pi^-$. We use $D^0 \to \pi^+ K^- \pi^+ \pi^-$ rather than $D^0 \to \pi^+ K^-$ because the phase-space of the K^- π^+ pair is similar for $\Lambda_c^+ \to p \pi^+ K^-$ and $D^0 \to \pi^+ K^- \pi^+ \pi^-$, but not for $D^0 \to \pi^+ K^-$. Since these decays are Cabibbo favored, they have high yields and are expected to have negligible CP asymmetries, which we assume are zero. The decay-rate CP asymmetry of $\Xi_c^+ \to \Sigma^+ h^+ h^-$ is

$$A_{CP}(\Xi_c^+ \to \Sigma^+ h^+ h^-) = A'_N(\Xi_c^+ \to \Sigma^+ h^+ h^-) - A'_N(\Lambda_c^+ \to \Sigma^+ h^+ h^-), \quad (7)$$

and that of $\Lambda_c^+ \to p h^+ h^-$ is

$$A_{CP}(\Lambda_c^+ \to p h^+ h^-) = A'_N(\Lambda_c^+ \to p h^+ h^-) - A'_N(\Lambda_c^+ \to p\pi^+ K^-) + A'_N(D^0 \to \pi^+ K^- \pi^+ \pi^-). \quad (8)$$

Subtracting the Λ_c^+ asymmetries cancels final-state-baryon detection asymmetries. Adding the D^0 asymmetry cancels K^- and π^+ detection asymmetries that the subtraction of $A'_N(\Lambda_c^+ \to p\pi^+ K^-)$ introduces. For the former, the distributions of the final-state baryon's c.m. frame momentum and $\cos\theta$ must be the same in the signal and control channels. For the latter, the same must be true of the kaon-pion pair. We apply kinematic weights to candidates in each control channel so that their distributions match those of their signal channel. We assume there is no asymmetry in detecting the h^+h^- pair from the Ξ_c^+ and Λ_c^+ decays, and assign a systematic uncertainty for this assumption. The measured values of $A'_N(\Xi_c^+ \to \Sigma^+ h^+ h^-)$ and $A'_N(\Lambda_c^+ \to p h^+ h^-)$ remained unexamined until the entire analysis procedure was finalized to avoid potential bias.

II. BELLE II DETECTOR AND SIMULATION

The Belle II detector [35], which is located at the SuperKEKB asymmetric-energy e^+e^- collider [36], has a cylindrical geometry and includes a tracking system comprising a two-layer silicon pixel detector (PXD) surrounded by a four-layer double-sided silicon strip detector (SVD) and a 56-layer central drift chamber (CDC), which also measures charged-particle energy loss. For the data used here, the second layer of the PXD covered only 15% of the azimuthal range. The symmetry axis of these detectors, the z axis, is nearly coincident with the direction of the electron beam. Outside the CDC is a time-of-propagation detector (TOP) in the barrel region and an aerogel-based ring-imaging Cherenkov detector (ARICH) in the forward end cap. They provide information for charged-particle identification together with the energy loss measurements from the SVD and CDC. Surrounding the TOP and ARICH is an electromagnetic calorimeter (ECL) based on CsI(Tl) crystals that measures the energy deposited by photons, charged particles, K_L^0, and neutrons. Outside the ECL is a superconducting solenoid magnet that provides a 1.5 T field parallel to the z axis. Its flux return is instrumented with resistive-plate chambers and plastic scintillator modules to detect muons, K_L^0, and neutrons.

We use simulated events to identify sources of background, optimize candidate selection, weight control modes, determine fit models, and validate the analysis procedure. We generate $e^+e^- \to q\bar{q}$, where $q = u, d, s, c$, with KKMC [37], hadronize quarks with PYTHIA 8 [38], generate $\Upsilon(4S) \to B\bar{B}$ events and particle decay with EvtGen [39] and PYTHIA 8, and simulate detector response with Geant4 [40]. Beam-induced backgrounds are accounted for by including randomly triggered data. Both simulated and real data are reconstructed with the Belle II analysis software framework [41,42].

III. CANDIDATE SELECTION

Each charged particle must be associated with at least one hit in the CDC and have a distance of closest approach to the e^+e^- interaction point (IP) of less than 3 cm in z and 1 cm in the perpendicular plane. We identify charged particles as pions, kaons, or protons using information from all subdetector systems except the PXD [43]. A proton is identified using the likelihood of its track to be from a proton divided by the sum of likelihoods for it to be from a proton, kaon, or pion. Pions and kaons are identified using neural-network trained particle-identification probabilities. Σ^+ candidates are reconstructed via $\Sigma^+ \to p\pi^0$ and π^0 via $\pi^0 \to \gamma\gamma$.

A kinematic-vertex fit constrains the final-state particles' origin points and four-momenta to be consistent with the decay topology, the masses of the Σ^+ and π^0 candidates to be their known values [13], and the initial-state baryon to originate from the IP [44]. Only candidates with fit χ^2 probabilities greater than 0.001 are retained for subsequent analysis. Backgrounds due to random combinations of final-state particles and due to charmed baryons originating from decays of B mesons are reduced by restricting the initial-state baryon's c.m.-frame momentum and flight significance—the displacement vector from the IP to the decay vertex position, projected onto the momentum direction, divided by its uncertainty.

We optimize selection criteria by maximizing $S/\sqrt{S+B}$, where S and B are the signal and background yields determined from the fit described in Sec. IV in a signal channel in data in the region around the known initial-state baryon mass [13]. As a result $\Xi_c^+ \to \Sigma^+\pi^+\pi^-$ decays, which have a smaller rate and feature larger expected backgrounds, are selected with tighter requirements than $\Xi_c^+ \to \Sigma^+ K^+ K^-$ decays. For each control channel, we use the same criteria as for its corresponding signal channel.

A. $\Xi_c^+ \to \Sigma^+ h^+ h^-$ and $\Lambda_c^+ \to \Sigma^+ h^+ h^-$

We reconstruct each $\Xi_c^+ \to \Sigma^+ h^+ h^-$ or $\Lambda_c^+ \to \Sigma^+ h^+ h^-$ candidate from two oppositely charged particles and one Σ^+ candidate. Protons are identified with 92% efficiency and 5% kaon-as-proton and 0.3% pion-as-proton misidentification rates. Kaons and pions are identified with 89% and 98% efficiencies, respectively, with corresponding pion-as-kaon and kaon-as-pion misidentification rates of 7% and 24%.

Photon candidates are formed from clusters of energy deposition in the ECL that are not associated with a reconstructed charged particle. Each cluster must be in a region covered also by the CDC and have energy greater than 80 MeV if in the ECL's forward end cap, 30 MeV if in its barrel, and 60 MeV if in its backward end cap. Background photons are rejected using two multivariate classifiers that determine if a cluster is due to beam-induced background or a hadronic shower [45]. They use shower-related variables, the time difference between the e^+e^- collision and the cluster signal, and other information related to photon detection. A photon pair with mass in $[120, 145]$ MeV$/c^2$ is accepted as a neutral pion candidate.

A $p\pi^0$ pair with mass in $[1.166, 1.211]$ GeV$/c^2$ is accepted as a Σ^+ candidate; the mass resolution is 7 MeV$/c^2$. For $\Sigma^+K^+K^-$, the Σ^+ flight significance must be above 8 and the initial-state baryon must have c.m.-frame momentum above 2.4 GeV$/c$ and flight significance above -1.5. For $\Sigma^+\pi^+\pi^-$, the Σ^+ flight significance must be above 16 and the initial-state baryon must have c.m.-frame momentum above 2.7 GeV$/c$ and flight significance above 3.6.

B. $\Lambda_c^+ \to ph^+h^-$ and $\Lambda_c^+ \to p\pi^+K^-$

We reconstruct each $\Lambda_c^+ \to ph^+h^-$ or $\Lambda_c^+ \to p\pi^+K^-$ candidate from one proton candidate and two oppositely charged particles. Protons are identified with 90% efficiency, with 2% kaon-as-proton and 0.1% pion-as-proton misidentification rates. Kaons and pions are identified with 79% and 90% efficiencies, respectively, with corresponding pion-as-kaon and kaon-as-pion misidentification rates of 2% and 7%.

For pK^+K^-, the Λ_c^+ must have c.m.-frame momentum above 2.3 GeV$/c$ and flight significance above -0.75. For $p\pi^+\pi^-$, the Λ_c^+ must have c.m.-frame momentum above 2.5 GeV$/c$ and flight significance above 2.0. For $pK^-\pi^+$, the Λ_c^+ candidate must satisfy the same momentum and flight-significance requirements as the signal channel its asymmetry is being subtracted from.

C. $D^0 \to \pi^+K^-\pi^+\pi^-$

We reconstruct each $D^0 \to \pi^+K^-\pi^+\pi^-$ candidate from four charged particles with zero net charge. Charged pion and kaon candidates must satisfy the same pion and kaon criteria as for $\Lambda_c^+ \to ph^+h^-$. The D^0 candidate must have c.m.-frame momentum above 2.3 GeV$/c$, mass in $[1.8, 1.92]$ GeV$/c^2$, and χ^2 probability above 0.001 for a kinematic-vertex fit that constrains its momentum to point back to the IP. Due to the very large yield of the $D^0 \to \pi^+K^-\pi^+\pi^-$ control mode, we randomly select 10% of D^0 candidates to use for the asymmetry determination.

IV. YIELD AND ASYMMETRY DETERMINATION

We determine the asymmetries from the yields of the signal and control channels, separated into the forward and backward regions and by charge, by maximizing extended likelihoods of the unbinned mass distributions of the selected decay candidates. Simultaneous fits are performed for each pair of signal and corresponding charmed-baryon control channels, separated by charge, and for the forward and backward regions. The likelihoods parametrize two sources of candidates, correctly reconstructed ones and background; the number of misreconstructed candidates is negligible according to simulation.

We model each channel's correct-candidate distribution with a double-sided Crystal Ball function [46,47], with its parameters fixed to values determined from fits to simulated data integrated over the forward and backward regions. We model each channel's background distribution with a straight line with its parameters free. The yields of correctly reconstructed candidates and background are free.

For the correct-candidate models of each pair of signal channel and charmed-baryon control channel, we add two free parameters to account for a potential common offset and a potential common scaling of widths from the values determined from fits to simulated data. They are predominantly determined from the high-yield control modes. We add a mode offset and width scaling for the $D^0 \to \pi^+K^-\pi^+\pi^-$ channels as well, determined independently from the charmed-baryon channels.

The kinematic weights for the $\Lambda_c^+ \to \Sigma^+h^+h^-$ and $\Lambda_c^+ \to p\pi^+K^-$ control channels are calculated from the momentum and $\cos\theta$ distributions of the final-state proton. The weights for the $D^0 \to \pi^+K^-\pi^+\pi^-$ control channel are calculated from the momentum and $\cos\theta$ distributions of the kaon. Weighting in these distributions is sufficient to also equalize the Σ^+ and π^+ momentum and $\cos\theta$ distributions. We use the sPlot technique [48] to isolate the correct-candidate distributions, using the results of the yield fits. We first calculate weights to equalize the momentum distributions, apply those weights, and then calculate weights to equalize the $\cos\theta$ distributions. Figures 1–3 show these distributions with and without weighting. Small deviations remain in the momentum distributions, but the effect on the cancelation of detection asymmetries is negligible.

We then repeat the fits with the weighting to determine the yields and the asymmetries of the control modes. Figures 4 and 5 show the mass distributions of the candidates for each decay channel, the results of the final fit, and the resulting averaged yield asymmetries as functions of the masses. Table I lists the measured yields and forward, backward, and averaged yield asymmetries. The measured asymmetries in data sidebands, which indicate the amount of asymmetry due to backgrounds, agree with the simulation and are compatible with zero.

We validate this procedure by fitting to simulated distributions generated by sampling from models fit to the real data, and with different input asymmetry values. We find no biases.

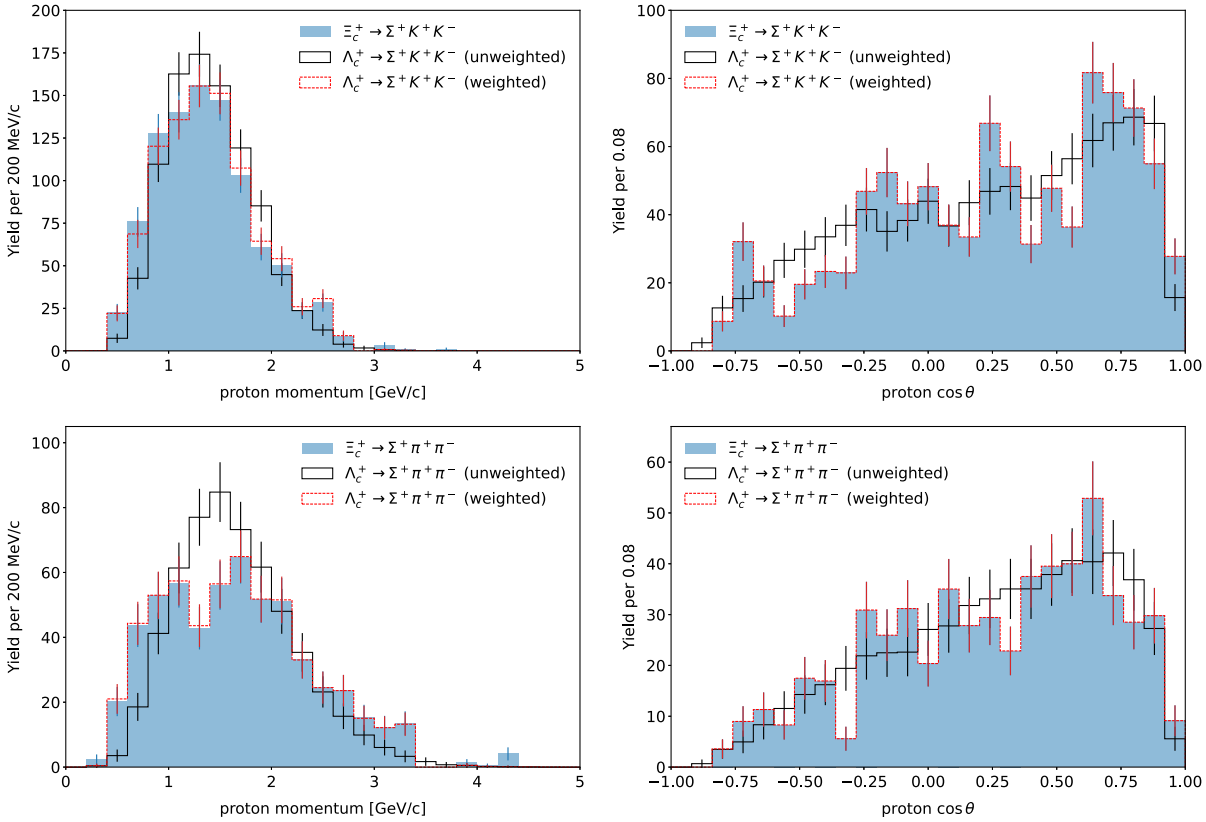

FIG. 1. Weighted and unweighted correct-candidate proton momentum (left) and $\cos\theta$ (right) distributions for $\Xi_c^+ \to \Sigma^+K^+K^-$ and $\Lambda_c^+ \to \Sigma^+K^+K^-$ (top) and $\Xi_c^+ \to \Sigma^+\pi^+\pi^-$ and $\Lambda_c^+ \to \Sigma^+\pi^+\pi^-$ (bottom).

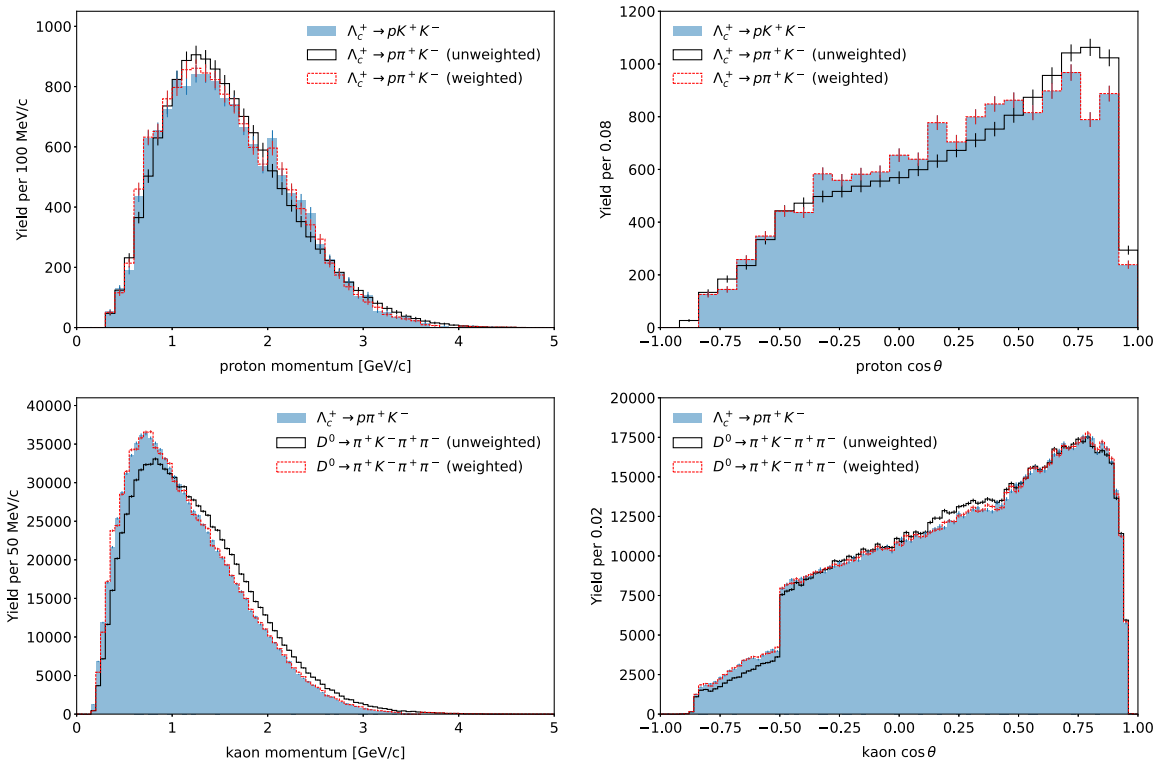

FIG. 2. Weighted and unweighted correct-candidate proton momentum (left) and $\cos\theta$ (right) distributions for $\Lambda_c^+ \to pK^+K^-$ and $\Lambda_c^+ \to p\pi^+K^-$ (top) and $\Lambda_c^+ \to p\pi^+K^-$ and $D^0 \to \pi^+K^-\pi^+\pi^-$ (bottom) with selection criteria for $\Lambda_c^+ \to pK^+K^-$.

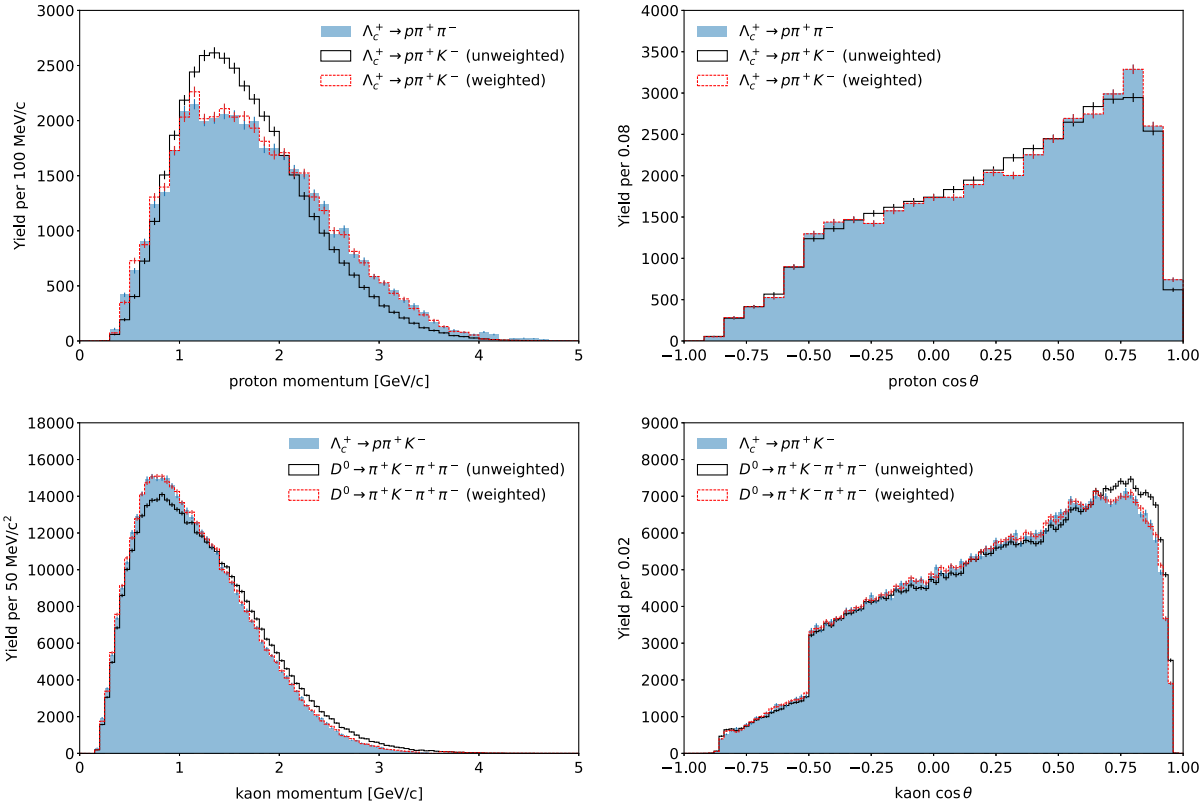

FIG. 3. Weighted and unweighted correct-candidate proton momentum (left) and cos θ (right) distributions for $\Lambda_c^+ \to p\pi^+\pi^-$ and $\Lambda_c^+ \to p\pi^+K^-$ (top) and $\Lambda_c^+ \to p\pi^+K^-$ and $D^0 \to \pi^+K^-\pi^+\pi^-$ (bottom) with selection criteria for $\Lambda_c^+ \to p\pi^+\pi^-$.

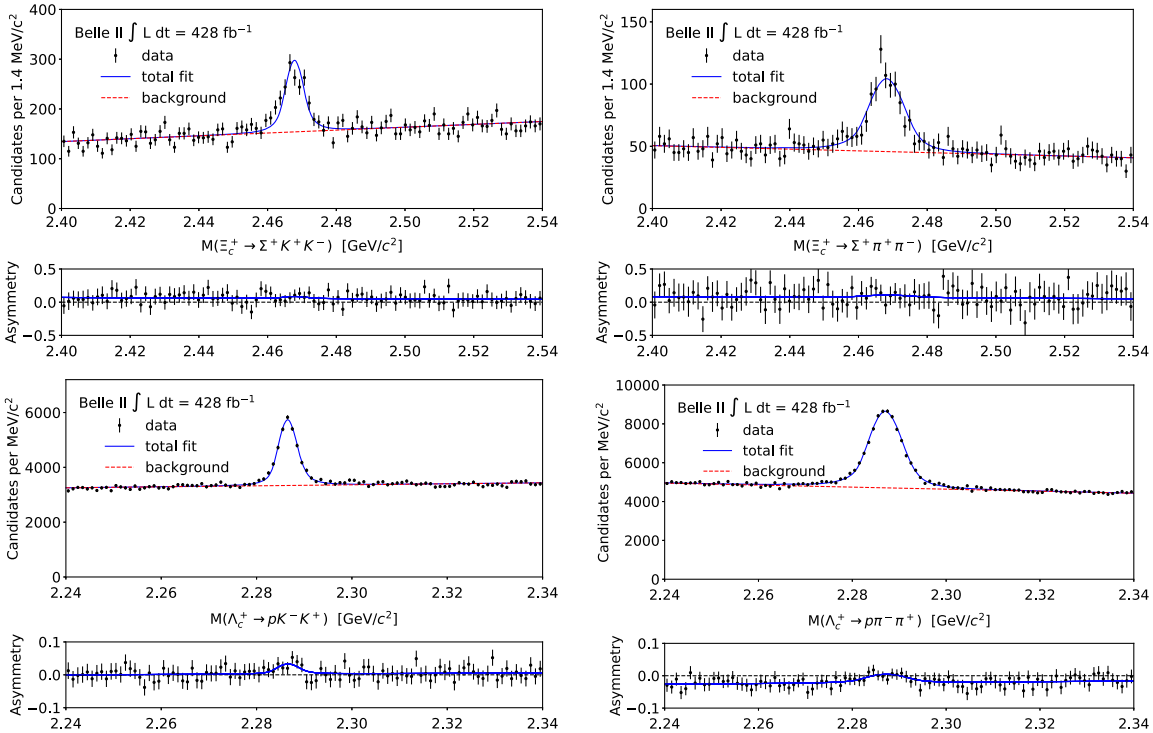

FIG. 4. Mass distributions for $\Xi_c^+ \to \Sigma^+h^+h^-$ (top) and $\Lambda_c^+ \to ph^+h^-$ (bottom) candidates for $h = K$ (left) and π (right) and the results of the fits, summing Ξ_c^+ and $\bar{\Xi}_c^-$ contributions and summing forward and backward contributions; and their averaged yield asymmetries as functions of mass, with fit projection overlaid.

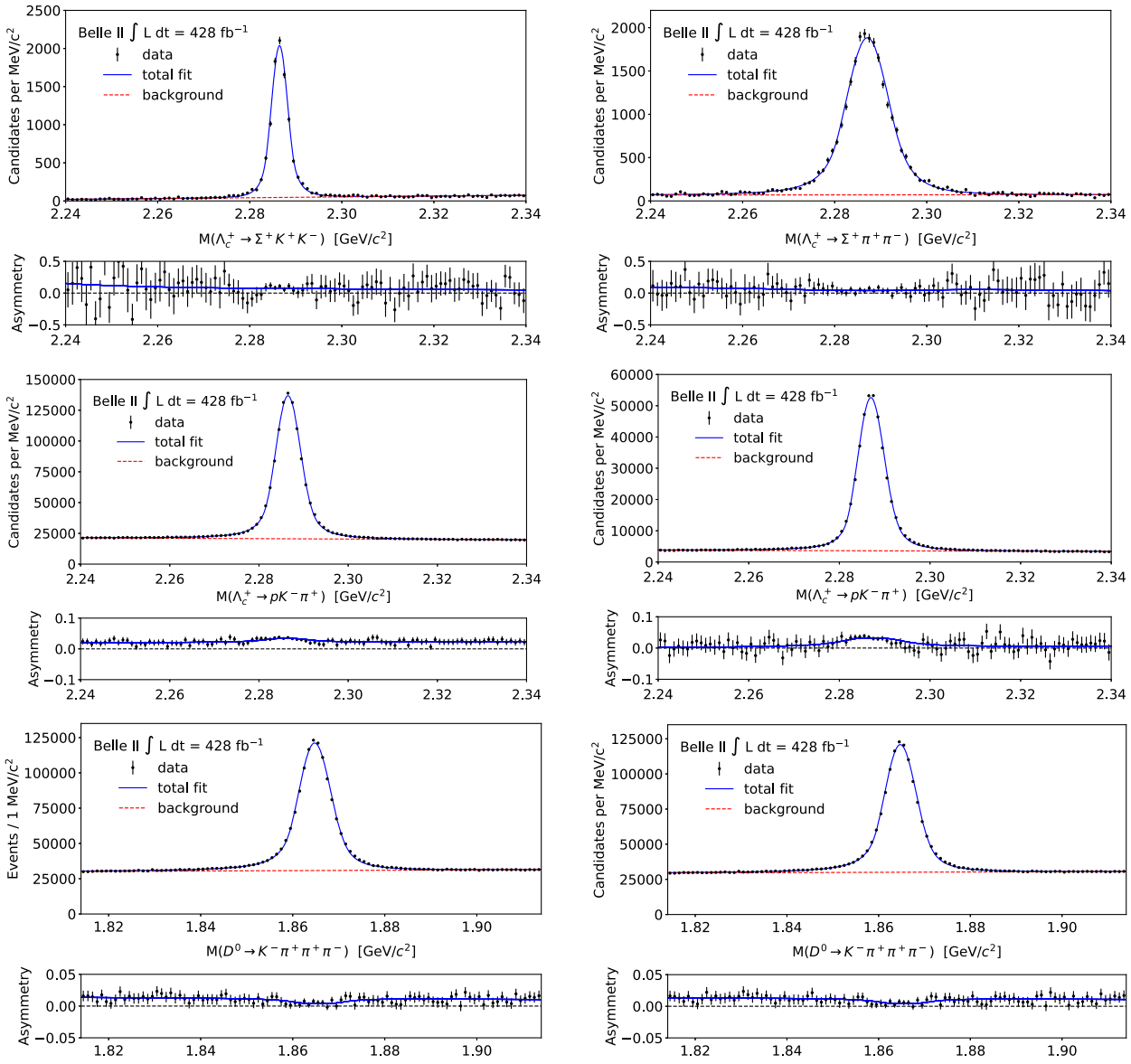

FIG. 5. Mass distributions for $\Lambda_c^+ \to \Sigma^+ h^+ h^-$ (top), $\Lambda_c^+ \to p\pi^+ K^-$ (middle), and $D^0 \to \pi^+ K^- \pi^+ \pi^-$ (bottom) candidates with the selection criteria for $\Lambda_c^+ \to pK^+ K^-$ (left) and $\Lambda_c^+ \to p\pi^+ \pi^-$ (right) and the results of the fits, summing Λ_c^+ and $\bar{\Lambda}_c^-$ contributions and summing forward and backward contributions; and their averaged yield asymmetries as functions of mass, with fit projection overlaid.

TABLE I. Yields (in 10^3) and asymmetries (in %) with statistical uncertainties.

Decay mode	Yield	Forward A_N	Backward A_N	A'_N
$\Xi_c^+ \to \Sigma^+ K^+ K^-$	0.78 ± 0.05	13.0 ± 9.2	10.5 ± 9.2	11.7 ± 6.5
$\Lambda_c^+ \to \Sigma^+ K^+ K^-$	9.9 ± 0.1	10.9 ± 1.5	5.3 ± 1.6	8.1 ± 1.1
$\Xi_c^+ \to \Sigma^+ \pi^+ \pi^-$	0.62 ± 0.04	17.0 ± 10.0	9.7 ± 8.9	13.3 ± 6.8
$\Lambda_c^+ \to \Sigma^+ \pi^+ \pi^-$	23.4 ± 0.2	7.4 ± 1.0	0.2 ± 1.0	3.8 ± 0.8
$\Lambda_c^+ \to pK^+ K^-$	13.6 ± 0.2	9.3 ± 2.2	5.5 ± 2.4	7.4 ± 1.7
$\Lambda_c^+ \to p\pi^+ K^-$[a]	955.0 ± 1.3	5.6 ± 0.2	1.6 ± 0.2	3.6 ± 0.1
$D^0 \to \pi^+ K^- \pi^+ \pi^-$[a]	928.0 ± 1.4	1.6 ± 0.2	-1.5 ± 0.2	0.1 ± 0.2
$\Lambda_c^+ \to p\pi^+ \pi^-$	40.5 ± 0.4	5.8 ± 1.3	1.5 ± 1.4	3.6 ± 0.9
$\Lambda_c^+ \to p\pi^+ K^-$[b]	410.3 ± 0.7	5.4 ± 0.3	1.5 ± 0.3	3.4 ± 0.2
$D^0 \to \pi^+ K^- \pi^+ \pi^-$[b]	925.2 ± 1.4	1.6 ± 0.2	-1.3 ± 0.2	0.1 ± 0.2

[a]Candidates are selected and kinematically weighted for the $\Lambda_c^+ \to pK^+ K^-$ mode.
[b]Candidates are selected and kinematically weighted for the $\Lambda_c^+ \to p\pi^+ \pi^-$ mode.

V. SYSTEMATIC UNCERTAINTIES

We repeat the fits to determine yields using a sum of Johnson's S_U function [49] and a Gaussian function in place of the double-sided Crystal Ball function for correct candidates and a second-order polynomial in place of the straight line for background (each separately). The results are consistent and we take the differences in quadrature of the asymmetry uncertainties as systematic uncertainties from the choice of the fit model.

We repeat the analysis with candidate weights using truth-matched candidates in simulation instead of using sPlot. We take the changes in results as systematic uncertainties arising from the weighting scheme. We also try determining the weights to equate the transverse-momentum distributions instead of the full-momentum distributions; the results change negligibly.

Since the detector acceptance depends on $\cos\theta$, a detection asymmetry due to the forward-backward asymmetry of charmed-baryon production may remain after averaging the forward and backward asymmetries. We estimate its effect by comparing the results of analyzing simulated data with and without candidates weighted to have identical $|\cos\theta|$ distributions for correct candidates (isolated using sPlot) in the forward and backward regions. The results are consistent. We take the differences as systematic uncertainties arising from potentially imperfect cancellation of $A_{\rm p}$. We also compared the results of analyzing real data with and without weights, determined according to the same weight function as for simulated data, and found consistent values.

We assumed there is no asymmetry in detecting the h^+h^- pair from the Ξ_c^+ and Λ_c^+ decays. To estimate the effects of such asymmetries, which may arise from intermediate states in the decays, we analyze data simulated to have exaggerated differences (compared to the real data) in the h^+ and h^- momentum distributions. The relative difference in average momentum of the two hadrons before and after modification ranges from 8% to 17%, depending on the channel. We take the differences in quadrature of the asymmetry uncertainties with and without this modification as systematic uncertainties due to a potential h^+h^- detection asymmetry, $A_{\rm d}(h^+h^-)$.

We have also assumed there is no asymmetry in detecting the $\pi^+\pi^-$ pair in the D^0 decay. To estimate the effect of such an asymmetry, we compare the yield asymmetries in data for $D^0 \to \pi^+K^-\pi^+\pi^-$ and $D^0 \to \pi^+K^-$, with the candidates of the four-body decay weighted so that the momentum and $\cos\theta$ distributions of its kaon and a randomly selected π^+ match those of the two-body decay. The weighted yield asymmetry for the four-body decay, $(-1.1 \pm 0.8)\%$, is consistent with that of the two-body decay, $(-0.4 \pm 0.2)\%$, showing that resonant structure in $D^0 \to \pi^+K^-\pi^+\pi^-$ does not significantly bias the subtraction of the π^+K^- detection asymmetry. We assign no systematic uncertainty for this potential effect.

TABLE II. Uncertainties on A_{CP} (in %).

Source	Ξ_c^+		Λ_c^+	
	$\Sigma^+K^+K^-$	$\Sigma^+\pi^+\pi^-$	pK^+K^-	$p\pi^+\pi^-$
Fit model	0.4	0.4	0.4	0.1
Weighting	0.1	0.2	0.3	0.1
Residual $A_{\rm p}$	0.2	0.1	0.1	0.1
$A_{\rm d}(h^+h^-)$	0.4	0.2	0.4	0.1
Total systematic	0.6	0.5	0.7	0.2
Statistical	6.6	6.8	1.7	1.0

Table II lists these systematic uncertainties, their quadrature sum, and the statistical uncertainties for each signal decay mode.

VI. RESULTS AND CONCLUSIONS

Using 428 fb^{-1} of e^+e^- collisions collected by Belle II, we measure

$$A_{CP}(\Xi_c^+ \to \Sigma^+K^+K^-) = (3.7 \pm 6.6 \pm 0.6)\%, \quad (9)$$

$$A_{CP}(\Xi_c^+ \to \Sigma^+\pi^+\pi^-) = (9.5 \pm 6.8 \pm 0.5)\%, \quad (10)$$

$$A_{CP}(\Lambda_c^+ \to pK^+K^-) = (3.9 \pm 1.7 \pm 0.7)\%, \quad (11)$$

$$A_{CP}(\Lambda_c^+ \to p\pi^+\pi^-) = (0.3 \pm 1.0 \pm 0.2)\%, \quad (12)$$

where the first uncertainties are statistical and the second ones systematic. These results agree with CP symmetry. Their U-spin sums are

$$A_{CP}(\Xi_c^+ \to \Sigma^+\pi^+\pi^-) + A_{CP}(\Lambda_c^+ \to pK^+K^-) = (13.4 \pm 7.0 \pm 0.9)\%, \quad (13)$$

$$A_{CP}(\Xi_c^+ \to \Sigma^+K^+K^-) + A_{CP}(\Lambda_c^+ \to p\pi^+\pi^-) = (4.0 \pm 6.6 \pm 0.7)\%, \quad (14)$$

consistent with U-spin symmetry. These are the world's first A_{CP} measurements for individual hadronic three-body charmed-baryon decays. Their uncertainties are predominantly statistical in origin, so future measurements using more data collected by Belle II will be important for precisely searching for CP violation and testing U-spin sum rules.

ACKNOWLEDGMENTS

This work, based on data collected using the Belle II detector, which was built and commissioned prior to March 2019, was supported by Higher Education and

Science Committee of the Republic of Armenia Grant No. 23LCG-1C011; Australian Research Council and Research Grants No. DP200101792, No. DP210101900, No. DP210102831, No. DE220100462, No. LE210100098, and No. LE230100085; Austrian Federal Ministry of Education, Science and Research, Austrian Science Fund (FWF) [Grants DOI: 10.55776/P34529, DOI: 10.55776/J4731, DOI: 10.55776/J4625, DOI: 10.55776/M3153, and DOI: 10.55776/PAT1836324], and Horizon 2020 ERC Starting Grant No. 947006 "InterLeptons"; Natural Sciences and Engineering Research Council of Canada, Digital Research Alliance of Canada, and Canada Foundation for Innovation; National Key R&D Program of China under Contract No. 2024YFA1610503, and No. 2024YFA1610504; National Natural Science Foundation of China and Research Grants No. 11575017, No. 11761141009, No. 11705209, No. 11975076, No. 12135005, No. 12150004, No. 12161141008, No. 12405099, No. 12475093, and No. 12175041, and Shandong Provincial Natural Science Foundation Project ZR2022JQ02; the Czech Science Foundation Grant No. 22-18469S, Regional funds of EU/MEYS: OPJAK FORTE CZ.02.01.01/00/22_008/0004632 and Charles University Grant Agency Project No. 246122; European Research Council, Seventh Framework PIEF-GA-2013-622527, Horizon 2020 ERC-Advanced Grants No. 267104 and No. 884719, Horizon 2020 ERC-Consolidator Grant No. 819127, Horizon 2020 Marie Sklodowska-Curie Grant Agreement No. 700525 "NIOBE" and No. 101026516, and Horizon 2020 Marie Sklodowska-Curie RISE project JENNIFER2 Grant Agreement No. 822070 (European grants); L'Institut National de Physique Nucléaire et de Physique des Particules (IN2P3) du CNRS and L'Agence Nationale de la Recherche (ANR) under Grant No. ANR-23-CE31-0018 (France); BMFTR, DFG, HGF, MPG, and AvH Foundation (Germany); Department of Atomic Energy under Project Identification No. RTI 4002, Department of Science and Technology, and UPES SEED funding Programs No. UPES/R&D-SEED-INFRA/17052023/01 and No. UPES/R&D-SOE/20062022/06 (India); Israel Science Foundation Grant No. 2476/17, U.S.-Israel Binational Science Foundation Grant No. 2016113, and Israel Ministry of Science Grant No. 3-16543; Istituto Nazionale di Fisica Nucleare and the Research Grants BELLE2, and the ICSC—Centro Nazionale di Ricerca in High Performance Computing, Big Data and Quantum Computing, funded by European Union—NextGenerationEU; Japan Society for the Promotion of Science, Grant-in-Aid for Scientific Research Grants No. 16H03968, No. 16H03993, No. 16H06492, No. 16K05323, No. 17H01133, No. 17H05405, No. 18K03621, No. 18H03710, No. 18H05226, No. 19H00682, No. 20H05850, No. 20H05858, No. 22H00144, No. 22K14056, No. 22K21347, No. 23H05433, No. 26220706, and No. 26400255, and the Ministry of Education, Culture, Sports, Science, and Technology (MEXT) of Japan; National Research Foundation (NRF) of Korea Grants No. 2021R1-F1A-1064008, No. 2022R1-A2C-1003993, No. 2022R1-A2C-1092335, No. RS-2016-NR017151, No. RS-2018-NR031074, No. RS-2021-NR060129, No. RS-2023-00208693, No. RS-2024-00354342 and No. RS-2025-02219521, Radiation Science Research Institute, Foreign Large-Size Research Facility Application Supporting project, the Global Science Experimental Data Hub Center, the Korea Institute of Science and Technology Information (K25L2M2C3) and KREONET/GLORIAD; Universiti Malaya RU grant, Akademi Sains Malaysia, and Ministry of Education Malaysia; Frontiers of Science Program Contracts No. FOINS-296, No. CB-221329, No. CB-236394, No. CB-254409, and No. CB-180023, and SEP-CINVESTAV Research Grant No. 237 (Mexico); the Polish Ministry of Science and Higher Education and the National Science Center; the Ministry of Science and Higher Education of the Russian Federation and the HSE University Basic Research Program, Moscow; University of Tabuk Research Grants No. S-0256-1438 and No. S-0280-1439 (Saudi Arabia), and Researchers Supporting Project number (RSPD2025R873), King Saud University, Riyadh, Saudi Arabia; Slovenian Research Agency and Research Grants No. J1-50010 and No. P1-0135; Ikerbasque, Basque Foundation for Science, State Agency for Research of the Spanish Ministry of Science and Innovation through Grant No. PID2022-136510NB-C33, Spain, Agencia Estatal de Investigacion, Spain Grant No. RYC2020-029875-I and Generalitat Valenciana, Spain Grant No. CIDEGENT/2018/020; The Knut and Alice Wallenberg Foundation (Sweden), Contracts No. 2021.0174, No. 2021.0299, and No. 2023.0315; National Science and Technology Council, and Ministry of Education (Taiwan); Thailand Center of Excellence in Physics; TUBITAK ULAKBIM (Turkey); National Research Foundation of Ukraine, Project No. 2020.02/0257, and Ministry of Education and Science of Ukraine; the U.S. National Science Foundation and Research Grants No. PHY-1913789 and No. PHY-2111604, and the U.S. Department of Energy and Research Awards No. DE-AC06-76RLO1830, No. DE-SC0007983, No. DE-SC0009824, No. DE-SC0009973, No. DE-SC0010007, No. DE-SC0010073, No. DE-SC0010118, No. DE-SC0010504, No. DE-SC0011784, No. DE-SC0012704, No. DE-SC0019230, No. DE-SC0021274, No. DE-SC0021616, No. DE-SC0022350, No. DE-SC0023470; and the Vietnam Academy of Science and Technology (VAST) under Grants No. NVCC.05.02/25-25 and No. DL0000.05/26-27. These acknowledgements are not to be interpreted as an endorsement of any statement made by any of our institutes, funding

agencies, governments, or their representatives. We thank the SuperKEKB team for delivering high-luminosity collisions; the KEK cryogenics group for the efficient operation of the detector solenoid magnet and IBBelle on site; the KEK Computer Research Center for on-site computing support; the NII for SINET6 network support; and the raw-data centers hosted by BNL, DESY, GridKa, IN2P3, INFN, and the University of Victoria.

DATA AVAILABILITY

The data that support the findings of this article are not publicly available upon publication because it is not technically feasible and/or the cost of preparing, depositing, and hosting the data would be prohibitive within the terms of this research project. The data are available from the authors upon reasonable request.

[1] J. H. Christenson, J. W. Cronin, V. L. Fitch, and R. Turlay, Evidence for the 2π decay of the K_2^0 meson, Phys. Rev. Lett. **13**, 138 (1964).
[2] A. Alavi-Harati *et al.* (KTeV Collaboration), Observation of direct CP violation in $K_{S,L} \to \pi\pi$ decays, Phys. Rev. Lett. **83**, 22 (1999).
[3] A. Lai *et al.* (NA48 Collaboration), A precise measurement of the direct CP violation parameter $\mathrm{Re}(\epsilon'/\epsilon)$, Eur. Phys. J. C **22**, 231 (2001).
[4] B. Aubert *et al.* (*BABAR* Collaboration), Observation of CP violation in the B^0 meson system, Phys. Rev. Lett. **87**, 091801 (2001).
[5] K. Abe *et al.* (Belle Collaboration), Observation of large CP violation in the neutral B meson system, Phys. Rev. Lett. **87**, 091802 (2001).
[6] B. Aubert *et al.* (*BABAR* Collaboration), Observation of direct CP violation in $B^0 \to K^+\pi^-$ decays, Phys. Rev. Lett. **93**, 131801 (2004).
[7] Y. Chao *et al.* (Belle Collaboration), Evidence for direct CP violation in $B^0 \to K^+\pi^-$ decays, Phys. Rev. Lett. **93**, 191802 (2004).
[8] R. Aaij *et al.* (LHCb Collaboration), First observation of CP violation in the decays of B_s^0 mesons, Phys. Rev. Lett. **110**, 221601 (2013).
[9] R. Aaij *et al.* (LHCb Collaboration), Observation of CP violation in $B^\pm \to DK^\pm$ decays, Phys. Lett. B **712**, 203 (2012); **713**, 351(E) (2012).
[10] R. Aaij *et al.* (LHCb Collaboration), Observation of CP violation in charm decays, Phys. Rev. Lett. **122**, 211803 (2019).
[11] R. Aaij *et al.* (LHCb Collaboration), Measurement of the time-integrated CP asymmetry in $D^0 \to K^+K^-$ decays, Phys. Rev. Lett. **131**, 091802 (2023).
[12] R. Aaij *et al.* (LHCb Collaboration), Observation of charge-parity symmetry breaking in baryon decays, Nature (London) **643**, 1223 (2025).
[13] S. Navas *et al.* (Particle Data Group), Review of particle physics, Phys. Rev. D **110**, 030001 (2024).
[14] M. Chala, A. Lenz, A. V. Rusov, and J. Scholtz, ΔA_{CP} within the standard model and beyond, J. High Energy Phys. 07 (2019) 161.
[15] A. Dery and Y. Nir, Implications of the LHCb discovery of CP violation in charm decays, J. High Energy Phys. 12 (2019) 104.
[16] L. Calibbi, T. Li, Y. Li, and B. Zhu, Simple model for large CP violation in charm decays, B-physics anomalies, muon $g-2$ and dark matter, J. High Energy Phys. 10 (2020) 070.
[17] A. J. Buras, P. Colangelo, F. De Fazio, and F. Loparco, The charm of 331, J. High Energy Phys. 10 (2021) 021.
[18] A. Pich, E. Solomonidi, and L. Vale Silva, Final-state interactions in the CP asymmetries of charm-meson two-body decays, Phys. Rev. D **108**, 036026 (2023).
[19] A. Lenz, M. L. Piscopo, and A. V. Rusov, Two body non-leptonic D^0 decays from LCSR and implications for $\Delta a_{\mathrm{CP}}^{\mathrm{dir}}$, J. High Energy Phys. 03 (2024) 151.
[20] R. Sinha *et al.*, Implications of the evidence for direct CP violation in $D \to \pi^+\pi^-$ decays, arXiv:2505.24338.
[21] Y. Grossman and S. Schacht, The emergence of the $\Delta U = 0$ rule in charm physics, J. High Energy Phys. 07 (2019) 020.
[22] H.-Y. Cheng and C.-W. Chiang, Revisiting CP violation in $D \to PP$ and VP decays, Phys. Rev. D **100**, 093002 (2019).
[23] S. Schacht and A. Soni, Enhancement of charm CP violation due to nearby resonances, Phys. Lett. B **825**, 136855 (2022).
[24] I. Bediaga, T. Frederico, and P. C. Magalhães, Enhanced charm CP asymmetries from final state interactions, Phys. Rev. Lett. **131**, 051802 (2023).
[25] M. Gavrilova, Y. Grossman, and S. Schacht, Determination of the $D \to \pi\pi$ ratio of penguin over tree diagrams, Phys. Rev. D **109**, 033011 (2024).
[26] S. Schacht, A U-spin anomaly in charm CP violation, J. High Energy Phys. 03 (2023) 205.
[27] F. Buccella, M. Lusignoli, G. Miele, A. Pugliese, and P. Santorelli, Nonleptonic weak decays of charmed mesons, Phys. Rev. D **51**, 3478 (1995).
[28] Y. Grossman, A. L. Kagan, and Y. Nir, New physics and CP violation in singly Cabibbo suppressed D decays, Phys. Rev. D **75**, 036008 (2007).
[29] Y. Grossman and S. Schacht, U-spin sum rules for CP asymmetries of three-body charmed baryon decays, Phys. Rev. D **99**, 033005 (2019).
[30] D. Wang, Sum rules for CP asymmetries of charmed baryon decays in the $SU(3)_F$ limit, Eur. Phys. J. C **79**, 429 (2019).
[31] R. Aaij *et al.* (LHCb Collaboration), A measurement of the CP asymmetry difference in $\Lambda_c^+ \to pK^-K^+$ and $p\pi^-\pi^+$ decays, J. High Energy Phys. 03 (2018) 182.
[32] F. A. Berends, K. J. F. Gaemers, and R. Gastmans, α^3 contribution to the angular asymmetry in $e^+e^- \to \mu^+\mu^-$, Nucl. Phys. **B63**, 381 (1973).

[33] R. W. Brown, K. O. Mikaelian, V. K. Cung, and E. A. Paschos, Electromagnetic background in the search for neutral weak currents via $e^+e^- \to \mu^+\mu^-$, Phys. Lett. **43B**, 403 (1973).
[34] R. J. Cashmore, C. M. Hawkes, B. W. Lynn, and R. G. Stuart, The forward-backward asymmetry in $e^+e^- \to \mu^+\mu^-$ comparisons between the theoretical calculations at the one loop level in the Standard Model and with the experimental measurements, Z. Phys. C **30**, 125 (1986).
[35] T. Abe *et al.* (Belle II Collaboration), Belle II technical design report, arXiv:1011.0352.
[36] K. Akai, K. Furukawa, and H. Koiso, SuperKEKB collider, Nucl. Instrum. Methods Phys. Res., Sect. A **907**, 188 (2018).
[37] S. Jadach, B. F. L. Ward, and Z. Wąs, The precision Monte Carlo event generator KK for two-fermion final states in e^+e^- collisions, Comput. Phys. Commun. **130**, 260 (2000).
[38] T. Sjöstrand, S. Ask, J. R. Christiansen, R. Corke, N. Desai, P. Ilten, S. Mrenna, S. Prestel, C. O. Rasmussen, and P. Z. Skands, An introduction to PYTHIA 8.2, Comput. Phys. Commun. **191**, 159 (2015).
[39] D. J. Lange, The EvtGen particle decay simulation package, Nucl. Instrum. Methods Phys. Res., Sect. A **462**, 152 (2001).
[40] S. Agostinelli *et al.* (GEANT4 Collaboration), Geant4–A simulation toolkit, Nucl. Instrum. Methods Phys. Res., Sect. A **506**, 250 (2003).
[41] T. Kuhr *et al.* (Belle II Framework Software Group), The Belle II core software, Comput. Software Big Sci. **3**, 1 (2019).
[42] Belle II Collaboration, Belle II Analysis Software Framework (BASF2), 10.5281/zenodo.5574115.
[43] I. Adachi *et al.* (Belle II Collaboration), Charged-hadron identification at Belle II, Eur. Phys. J. C **85**, 1237 (2025).
[44] J.-F. Krohn *et al.* (Belle II Analysis Software Group), Global decay chain vertex fitting at Belle II, Nucl. Instrum. Methods Phys. Res., Sect. A **976**, 164269 (2020).
[45] P. Cheema, Suppressing beam background and fake photons at Belle II using machine learning, EPJ Web Conf. **295**, 09035 (2024).
[46] J. Gaiser, Charmonium spectroscopy from radiative decays of the J/ψ and ψ', Ph.D. thesis, Stanford University, 1982.
[47] T. Skwarnicki, A study of the radiative CASCADE transitions between the Upsilon-Prime and Upsilon resonances, Ph.D. thesis, INP, Cracow, 1986.
[48] M. Pivk and F. R. Le Diberder, sPlot: A statistical tool to unfold data distributions, Nucl. Instrum. Methods Phys. Res., Sect. A **555**, 356 (2005).
[49] N. L. Johnson, Systems of frequency curves generated by methods of translation, Biometrika **36**, 149 (1949).